International Journal of Heat and Mass Transfer 52 (2009) 5250–5257

Contents lists available at ScienceDirect

International Journal of Heat and Mass Transfer

journal homepage: www.elsevier.com/locate/ijhmt

Asymmetric entrainment effect on the local surface temperature of a flat plate heated by an obliquely impinging two-dimensional jet

O. Vipat [a,b], S.S. Feng [a], T. Kim [a,*], A.M. Pradeep [b], T.J. Lu [a,*]

[a] MOE Key Laboratory for Strength and Vibration, School of Aerospace, Xi'an Jiaotong University, Xi'an 710049, PR China
[b] Department of Aerospace Engineering, Indian Institute of Technology Bombay, Powai, Mumbai 400076, India

ARTICLE INFO

Article history:
Received 28 September 2008
Received in revised form 7 April 2009
Accepted 14 April 2009
Available online 8 June 2009

Keywords:
Asymmetric entrainment
Cold jet
Heated jet
Inclination
Two-dimensional jet

ABSTRACT

The flow and temperature fields caused by a two-dimensional heating air jet obliquely impinging on a flat plate are experimentally characterized. Whilst the jet flow is discharged at $Re_{Dh} = 8.2 \times 10^3$ based on the hydraulic diameter of the orifice, D_h, and the jet exit-to-plate spacing (separation distance) is fixed at $8D_h$, the impingement angle (inclination) is systematically decreased from 90° (normal impinging) to 30° (oblique impinging). A separate experiment is carried out for a two-dimensional cooling jet obliquely impinging on a heated plate (constant heat flux). The results demonstrate that the response of local surface temperature to plate inclination behaves in a completely different manner. For impinging jet cooling, the inclination (from normal impinging position) reduces the local effective temperature values at corresponding points about actual stagnation point, inclusive of it. For impinging jet heating, the inclination causes, conversely, an increase in local surface temperature including the stagnation point temperature. However, the shifting of the actual stagnation point towards the uphill side of the plate is consistently observed for both hot and cold jet cases. This newly found feature for an obliquely impinging jet is attributed to the combined effects of asymmetric entrainment and momentum redistribution (i.e., thickening/thinning of hydraulic boundary layers on each side of the plate with respect to the actual stagnation point).

1. Introduction

Impinging jets have been extensively used in various industrial fields such as paper drying, blade cooling and annealing of glass, and hence numerous studies (mainly experimental) have been carried out to explore the thermal and flow mechanisms associated with an impinging jet. Sparrow and Lovell [1] measured the heat and mass transfer coefficients for an obliquely impinging circular air jet (three-dimensional) on a heated flat plate. The effects of varying the inclination angle (from 90° to 30°), Reynolds number and jet-to-plate spacing were quantified. It was established that the point where maximum heat transfer occurs is shifted towards the uphill side of the target plate due to inclination. However, the averaged heat transfer coefficient is not highly sensitive to the inclination angle although the local distribution is. Beitelmal et al. [2] investigated an obliquely impinging slot (two-dimensional) air jet on a heated plate for Reynolds numbers (based on hydraulic diameter D_h of slot) varying in the range of 4.0×10^3–1.2×10^4, inclination angles varying from 90° (normal impinging) to 40°, and jet-to-plate spacing in the range of $4D_h$–$12D_h$. Similar to a circular jet, the location where maximum heat transfer occurs is found to shift uphill for a slot jet. It is also observed that the maximum Nusselt number decreases with increasing inclination angle (from normal impinging position).

The majority of previous studies [1–4] have focused on an unheated air jet impinging on a heated flat plate having either constant temperature or constant heat flux. For a heated jet, the jet exit temperature is higher than the temperatures of the ambient fluid and the target plate. This introduces additional complexity in heat transfer analysis because the entrainment of the (cold) ambient air plays a crucial part in determining the amount of heat transferred to the plate [5,6], although the flow field remains unchanged compared to a cold impinging jet (as observed in the present study).

Goldstein et al. [5] examined the effect of entrainment on a circular jet normally impinging on a flat plate for separation distances varying from $2D$ to $12D$, where D represents the circular jet diameter. It is concluded that, if the adiabatic wall temperature is known, then the heat transfer coefficient of a cooling jet can be used for a heated jet. For the latter, this can be represented by a new definition of the heat transfer coefficient incorporating the adiabatic wall temperature. The concept of effectiveness (which is widely used in film cooling) was adopted to characterize the entrainment using the recovery temperature introduced by Goldstein et al. [5]. It is found that for separation distances larger

* Corresponding authors.
E-mail addresses: tongbeum@gmail.com (T. Kim), tjlu@mail.xjtu.edu.cn (T.J. Lu).

0017-9310/$ - see front matter © 2009 Elsevier Ltd. All rights reserved.
doi:10.1016/j.ijheatmasstransfer.2009.04.007

Nomenclature

Cp	non-dimensional pressure coefficient defined in Eq. (2)
D	circular jet diameter (m)
D_h	hydraulic diameter of two-dimensional orifice (m)
p	pressure measured along selected lateral position on target plate (Pa)
p_{amb}	ambient pressure (Pa)
Re_{Dh}	Reynolds number based on hydraulic diameter defined in Eq. (1)
s	axis normal to target plate
T_{amb}	ambient temperature (K)
T_j	exit flow temperature measured at the exit center of two-dimensional orifice (K)
$T_{no\text{-}flow}$	uniform temperature on target plate (devoid of cooling jet impingement) (K)
T_s	local wall temperature on target plate (K)
u	wall jet velocity (m/s)
V	axial component of jet velocity (m/s)
V_m	jet exit mean velocity (m/s)
y	lateral axis along target plate
z	jet axis coinciding with jet center

Greek symbols

β	relative angle of two-dimensional orifice measured from the axis parallel to target plate (°)
θ	effective temperature defined in Eq. (3)
μ	viscosity of air (kg/ms)
ρ	density of air (kg/m^3)

than 4D, the entrainment of ambient air is an important factor which affects even the centerline temperature of the jet flow. Using an experimental setup similar to that of Goldstein et al. [5], Baughn et al. [6] calculated the effectiveness and Nusselt number for three selected separation distances, i.e., 2D, 6D and 10D, and concluded that even though the heat transfer coefficients (defined in terms of adiabatic wall temperature) could be used for a heated jet as well as a cooling jet, this does not mean the entrainment effects are negligible. Furthermore, the exact data obtained with a cooling jet can not be used in place of a heated jet due to entrainment effects in the latter.

Striegl and Diller [7] studied analytically a heated slot jet impinging on a flat plate by introducing a new parameter, the entrainment factor F, and proposed correlations for both the Nusselt number and the wall temperature. However, only normal impingement was considered. Perry [8] studied a circular hot jet impinging on a flat plate for various impinging angles and used a simple method to calculate the gross heat transfer between the jet and the plate.

Despite numerous previous studies on impinging jets, existing literature dealing with a heated oblique two-dimensional (slot) jet is scarce. This study aims therefore to squarely address this deficiency by investigating experimentally the effect of entrainment on a two-dimensional heated jet impinging on an unheated flat plate; for comparison, a cooling jet obliquely impinging on a heated flat plate (constant heat flux) is also studied. Particular focus is placed upon the asymmetric entrainment caused by inclination of the heated jet relative to the target plate and its influence on local temperature distribution on the plate. To simplify the problem, the jet-to-plate separation distance and the Reynolds number are fixed at $8D_h$ and 8.2×10^3, respectively, whilst the inclination angle is systematically varied from 90° (normal impinging) to 30° (oblique impinging).

2. Experimental setup

2.1. Test rig

The experimental setup is schematically shown in Fig. 1. Flow drawn by a centrifugal blower passes a settling chamber, followed by an orifice flow meter (for calculation of mean flow velocity). The orifice has a length of 88.6 mm and a width (denoted by b in Fig. 1) of 6.35 mm. Due to the large length-to-width ratio of the orifice (=14), the flow discharged from the orifice may be approximated as two-dimensional. To create the heated jet, air from the centrifugal fan is sent to the settling chamber, which is then directed to a heater before being discharged from the two-dimensional orifice.

The square Perspex target flat plate has width 200 mm and thickness 10 mm, and the thermal conductivity of its base material is $k \sim 0.2$ W/mK. The flat plate laterally spans from $y = -8.4D_h$ to $y = +8.4D_h$. The impinging side of the plate was painted in black to enhance the reflectivity for infrared thermography, whereas a thermal insulation material having the thermal conductivity of 0.032 W/mK and thickness of 0.05 m was attached to the back side of the plate. The angle of inclination, β, of the target plate can be varied from 30° to 90° (normal impinging position).

2.2. Pressure and velocity measurements

Pressure measurements on the target plate with an obliquely impinging jet were performed. A total of 15 flush mounted static pressure tappings were laterally distributed on the plate. Velocity measurements for the jet exit flow were conducted with a Pitot tube mounted on a linear traverse system. The measurements were carried out under free jet conditions (i.e., in the absence of the target plate). The lateral distribution of the axial jet flow velocity was obtained at five selected traverse planes: $z/D_h = 0$, 2, 4, 6, and 8. All the static pressure tappings and the Pitot tube were connected to a multi-channel differential pressure transducer to record the pressure measurements.

2.3. Temperature measurements

Two series of heat transfer measurements were carried out: (a) hot jet impingement; (b) cold jet impingement (as reference). For hot jet impingement, temperature data on the target plate were obtained using a pre-calibrated infrared camera positioned at an angle α from the jet centerline axis (z-axis), as illustrated in Fig. 1. The images were corrected for non-perpendicular viewing angles ($\pi/2 - \alpha$) during post-image processing. A T-type foil thermocouple, 20 μm thick, was used to measure the temperature at the geometrical stagnation point ($y = 0$). This thermocouple was also used to calibrate the infrared camera in situ. It is assumed that, due to the thin thickness of the foil thermocouple, it does not disturb the flow and temperature fields in the impinging jet. Additionally, two T-type bead thermocouples were used to measure the ambient and jet exit temperatures. A temperature scanner was used to record temperature values from these thermocouples.

For cold jet impingement, an etched foil heating pad having dimensions of 0.127 m (length) × 0.127 m (width) × 0.5 mm (thickness) was embedded inside the target plate and covered with a 5 μm thick aluminum foil, with the latter painted in black for enhanced reflectivity. Controlled by a DC power source, the heating

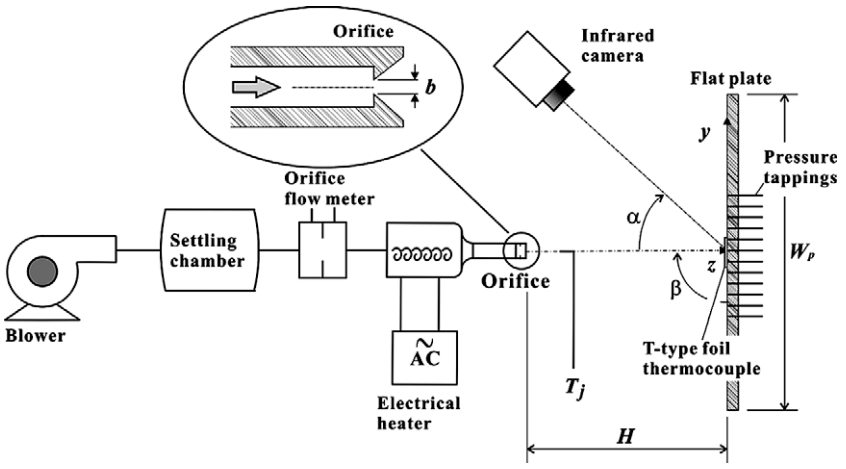

Fig. 1. Schematic of test setup for an impinging two-dimensional heated jet.

pad imposes a constant heat flux of approximately 0.88 kW/m^2 on the target plate.

2.4. Data reduction parameters

Jet Reynolds number based on the hydraulic diameter of the orifice, D_h, and jet exit mean velocity, V_m, calculated from the orifice flow meter is defined as:

$$\mathrm{Re}_{Dh} = \frac{\rho V_m D_h}{\mu} \tag{1}$$

For the present study, the jet Reynolds number is fixed at 8.2×10^3. To evaluate the distribution of static pressure on the surface of the plate, a non-dimensional pressure coefficient, C_p, is defined as:

$$C_p = \frac{p - p_{amb}}{\rho V_m^2/2} \tag{2}$$

where p is the pressure measured along the selected lateral position on the plate and p_{amb} is the ambient pressure.

Local heat transfer on the plate was evaluated using the Nusselt number Nu_{Dh} which, for the case of cold impinging jet, is defined as:

$$Nu_d = \left(\frac{q''}{(T_s(y/D_h) - T_{amb})}\right)\frac{D_h}{k_f} \tag{3}$$

where q'' is the heat flux imposed by the heating pad on the plate, $T_s(y/D)$ is the local surface temperature of the plate, and T_{amb} is the ambient temperature. To compare the wall temperature measured under a heating jet and that associated with a cooling jet, the effective temperature (θ) is defined as:

$$\theta = \frac{(T_{no\text{-}flow} - T_s - T_{amb})}{(T_{no\text{-}flow} - T_{amb})} \quad \text{for cold jet} \tag{4a}$$

$$\theta = \frac{(T_s - T_{amb})}{(T_j - T_{amb})} \quad \text{for heated jet} \tag{4b}$$

where $T_{no\text{-}flow}$ is the uniform temperature on the plate induced by the constant heat flux source in the absence of the cooling jet impingement, and T_j is the exit flow temperature measured at the exit center of the two-dimensional orifice. For the heated jet, the effective temperature used in the present study is similar to that defined in the literature [5,6].

Physically, the effective temperature may be understood as the effectiveness of the impinging jet transferring heat to/from the target plate. The jet effectiveness in the cooling case is indicated by the temperature to which the target plate is cooled with respect to the initial temperature. For the heating jet case, the effective temperature θ implies the effectiveness of the jet in heating the target plate. Another interpretation of θ may be the deviation of temperature on the target plate from that in the absence of impinging flow. Hence, θ values near 1 would mean that the wall temperature is near to the jet temperature whereas θ values near 0 would mean the wall temperature is near to its no flow value. Therefore, physically, the effective temperature has a meaning similar to that of the heat transfer coefficient.

2.5. Measurement uncertainty

The uncertainties associated with the present static pressure, velocity, pressure coefficient and temperature measurements were estimated using the method reported in Coleman and Steele [9] based on 20:1 odds. For pressure measurements, the maximum error occurs at $\beta = 30°$. The uncertainty associated with the wall pressure data and the corresponding pressure coefficient is calculated to be 2% and 3.25%, respectively, with the typical wall pressure being 25 ± 0.5 Pa. The uncertainty associated with the temperature difference is caused by errors in the wall temperature data measured by the infrared camera as well as in the ambient temperature measured by the T-type thermocouples. Calibration of the infrared camera and thermocouples performed prior to the temperature measurements showed that the combined error in the temperature difference is within 0.4 °C and the uncertainty in the typical operating conditions is thus found to be 0.65%. The uncertainty of the non-dimensional temperatures defined in Eq. (3) for the cold jet case is estimated to be 1.5%. Heat loss due to radiation was estimated to be negligible since the temperature difference between the cooling jet flow in ambient conditions and the heated plate was typically within 10 K. Systematic errors were minimized by careful calibrations and hence assumed negligible.

3. Discussion of results

3.1. Wall pressure distribution and flow characteristics

In the presence of an impinging hot jet flow, the lateral variation of pressure coefficient C_p defined in Eq. (2) on the target plate is shown in Fig. 2. The separation distance was fixed at $H/D_h = 8$, the nominal temperature difference between the ambient (T_{amb}) and the hot impinging jet (T_j) was kept at $T_j - T_{amb} \sim 45$ K, whilst the inclination angle measured from the axis parallel to the plate was decreased from 90° (normal impinging) to 30° (oblique

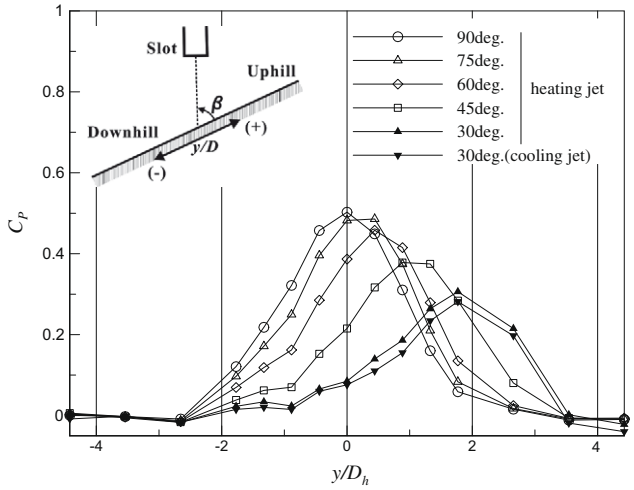

Fig. 2. Variation of surface pressure distribution with inclination for $H/D_h = 8$ and $Re_{Dh} = 8.2 \times 10^3$.

impinging) with a 15° increment. During the pressure measurements, the impinging jet flow was heated. In addition, at $\beta = 30°$, pressure data in the presence of a cold impinging jet were also acquired and included in Fig. 2 in order to examine a possible effect of heat input to the impinging jet flow on the distribution of local pressure.

For a normally impinging jet ($\beta = 90°$), the distribution of pressure coefficient (C_p) is laterally symmetric with respect to the geometrical stagnation point $y/D_h = 0$, which is also the center of the plate (Fig. 2). Whilst the highest pressure occurs at the geometrical stagnation point, the value of local C_p monotonically decreases away from the stagnation point till y/D_h reaches approximately 2.5. Further away, a sub-atmospheric region is present (Fig. 2) where the local pressure is lower than the ambient pressure, which is consistent with existing results [10].

As the inclination angle of the target plate is decreased from the normal impinging position, the peak value of C_p at the actual stagnation point is reduced from $C_p = 0.5$ for the case of $\beta = 90°$ to $C_p = 0.306$ for the $\beta = 30°$ case (Fig. 2). Furthermore, the shifting of the stagnation point towards a region called the "uphill side" (see the inset of Fig. 2) is clearly seen, consistent with the observation reported in reference [3]. Due to the uphill shift, the lateral distribution of C_p is no longer symmetric with respect to the geometrical stagnation point. At the same lateral distances from the geometrical stagnation point, the C_p values on the uphill side are higher than those on the downhill side.

The effect of a cold jet on wall pressure distribution is represented by an additional curve depicted in Fig. 2, which is measured at $\beta = 30°$ for a cold impinging jet of ambient temperature. The lateral distributions of local pressure for both the heating and cooling cases are nearly identical within the uncertainty associated with the present pressure coefficient measurement. This also suggests that the buoyancy effect in the hot jet is negligible for the nominal temperature difference (45 K) considered in the present study.

The static pressure distributions shown in Fig. 2 are induced by the impingement of jet flow discharged from a two-dimensional orifice (Fig. 1). It is therefore instructive to characterize the flow fields in the impinging jet. Fig. 3(a) displays the measured velocity profiles of the discharged flow in free jet conditions, traversed at five selected downstream planes: $z/D_h = 0$, 2, 4, 6, and 8. The velocity profiles are symmetric with respect to the jet axis (z-axis). It is inferred from Fig. 3(a) that the velocity is fully developed when $z/D_h = 8$. In the presence of a target plate (located at $z/D_h = 8$ in the present study), the flow fields plotted in Fig. 3(a) are expected to vary, especially those in the vicinity of the plate, but away from

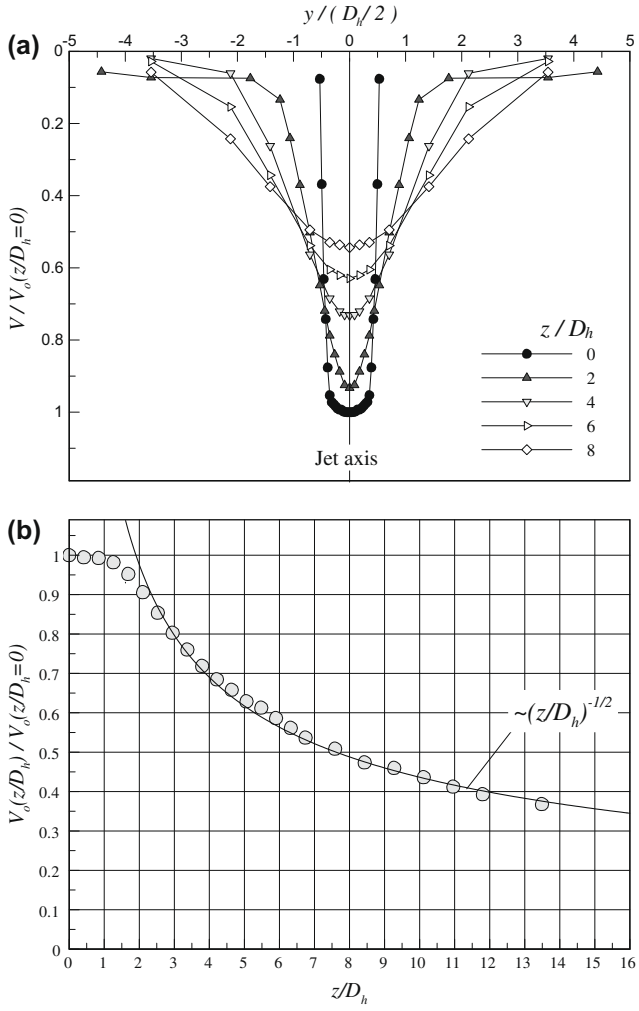

Fig. 3. Free slot jet velocity measurements at $Re_{Dh} = 8.2 \times 10^3$: (a) velocity profile and (b) axial variation of centerline velocity.

the plate the character of the flow fields should largely follow that exhibited in Fig. 3(a) for free jet flow. Hofmann et al. [11] observed that the presence of an impingement plate influences the jet flow structure only when the flow is approximately $1.0D_h$ or less from the plate; other flow regions towards the orifice remain unaffected.

To estimate the length of the potential core, axial velocity along the centerline, i.e., $y/D_h = 0$, was measured in free exit conditions and plotted in Fig. 3(b). The centerline velocity V_c is decreases substantially after $z/D_h \sim 1.5$, following a classical trend of $(z/D_h)^{-1/2}$. The axial variation of the centerline velocity along the z-axis suggests that the potential core lies within $2D_h$, which is typical of two-dimensional orifices [12].

The results of Figs. 2 and 3 on wall pressure distribution and jet flow fields establish the fact that the flow characteristics associated with a hot impinging jet are nearly identical to those of a cold jet. Furthermore, no irregularities of the jet flow characteristics (including the axial symmetry of velocity and pressure distributions, potential core length, and variation with inclination) are observed. Hence, the jet flow discharged from the present two-dimensional orifice (Fig. 1) is consistent with typical slot jet flows reported in references [3,13].

3.2. Heat transfer characteristics

After establishing the near similarity of the jet flow characteristics for heating and cooling jets, we analyze in detail the heat

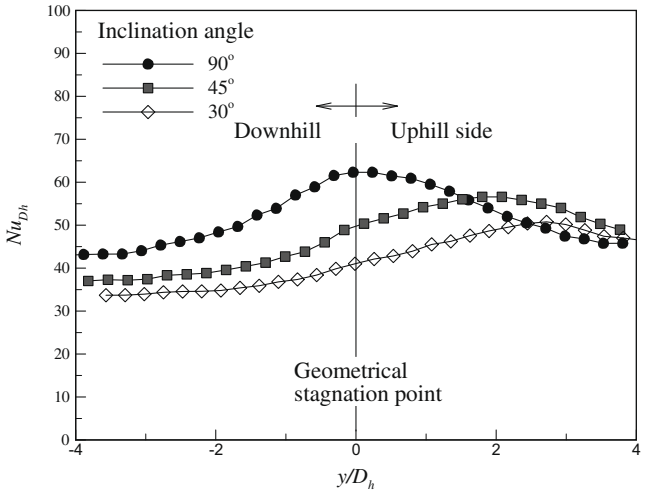

Fig. 4. Lateral distribution of Nusselt number for two-dimensional orifice cooling jet flow where $q'' = 0.88$ kW/m^2, $Re_{Dh} = 8.2 \times 10^3$, and $H/D_h = 8$.

transfer characteristics of the cold impinging jet; the measured results are shown in Fig. 4. The measurements were performed with the target plate maintained under constant heat flux for varying inclination angles, with the separation distance fixed at $8D_h$ and the Reynolds number Re_{Dh} at 8.2×10^3.

Figs. 4 and 5(a) plot separately the measured lateral distribution of Nusselt number and effective wall temperature θ as defined in Eq. (4a) for three selected inclination angles: 90°, 45° and 30°. The Nusselt number (or effective temperature) for $\beta = 90°$ (normal impingement) is maximized at the geometrical stagnation point ($y/D_h = 0$), and is symmetrically distributed with respect to this point. Analogous to the wall pressure coefficient C_p (Fig. 2), the actual stagnation point where maximum heat transfer occurs is shifted towards the uphill side as the plate inclination angle is decreased. The extent of the uphill shift appears to intensify with decreasing inclination angle (Fig. 5(a)). In addition to the shifting of the actual stagnation point, the results of Fig. 5(a) show that the Nusselt number (or effective temperature) of the plate on the uphill side is larger than that on the downhill side for the same lateral distance from the actual stagnation point. However, the rate at which the Nusselt number decreases as the lateral distance from the actual stagnation point is increased is steeper on the uphill side. Therefore, for a sufficiently large distance from $y/D_h = 0$ (e.g., data reported in references [2,3]), the effective temperature on the uphill side would become lower than that on the downhill side, although this is not observed in the lateral range ($y/D_h = \pm 4$) considered in the present study. Fig. 5(b) schematically illustrates such crossing inferred from the test data of Figs. 4 and 5(a) where the lateral distance of the crossing point from the geometrical stagnation point is $y_{c,up}/D_h > +4$ for the uphill side and $y_{c,down}/D_h < -4$ for the downhill side. The present observations are consistent with the results reported in [2,3].

Fig. 6(a) presents the lateral distribution of effective wall temperature θ for the hot impingement case, with the inclination angles selected as: 90°, 45° and 30°. For $\beta = 90°$, the effective temperature peaks at the geometrical stagnation point and the distribution is laterally symmetric relative to this point, with the temperature decreasing monotonically on either side. The trend is similar to that shown in Fig. 5(a) for the case of the $\beta = 90°$ cooling jet. Furthermore, it is seen from Fig. 6(a) that, with increment in inclination from the normal impingement, the actual stagnation point is shifted towards the uphill side of the target plate.

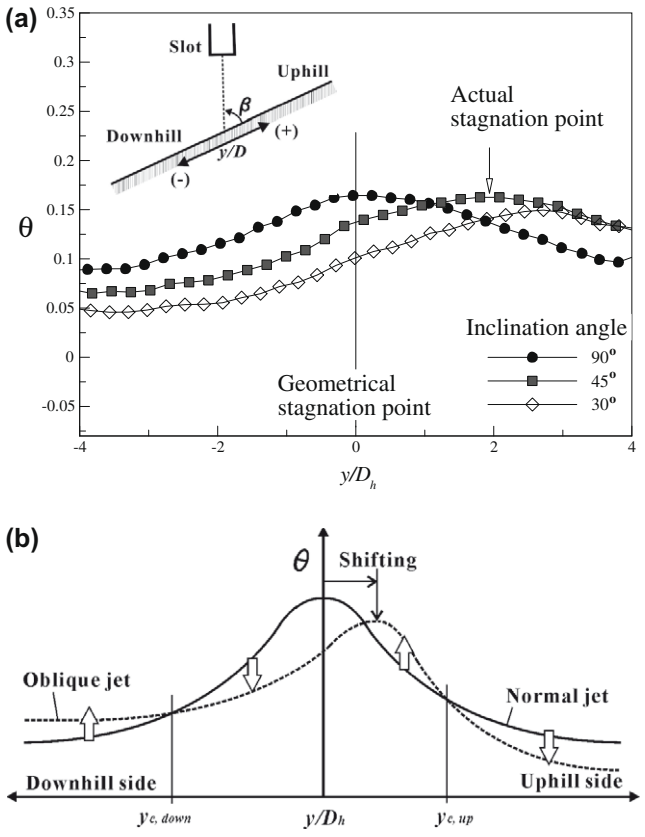

Fig. 5. Lateral distribution of effective wall temperature for two-dimensional orifice cooling jet flow: (a) measured data and (b) schematic variation of effective temperature with inclination.

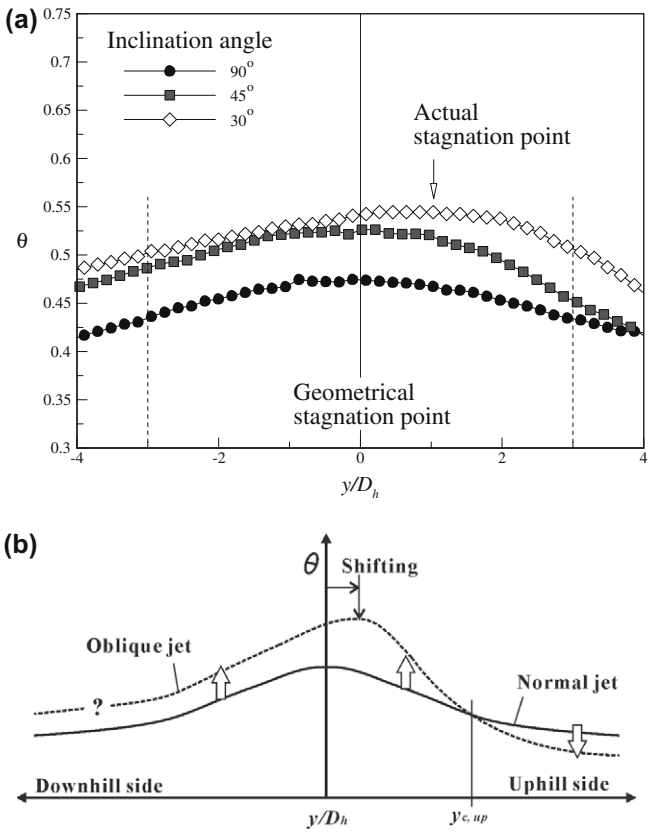

Fig. 6. Lateral distribution of effective wall temperature for two-dimensional orifice hot jet flow: (a) measured data and (b) schematic variation of effective temperature with inclination.

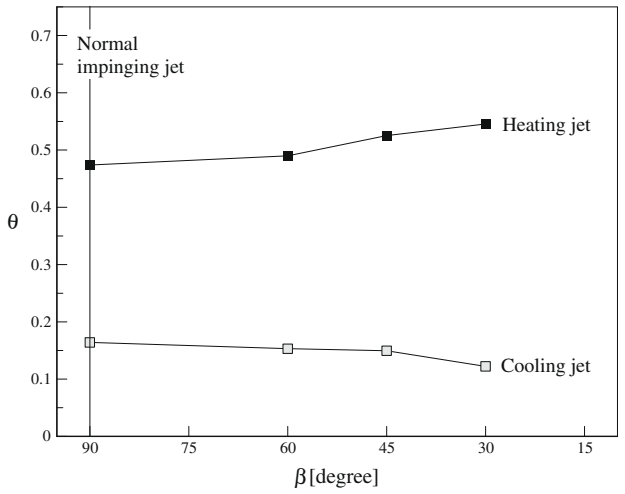

Fig. 7. Effective wall temperature at geometrical stagnation point ($y/D_h = 0$) plotted as a function of inclination angle for $Re_{Dh} = 8.2 \times 10^3$ and $H/D_h = 8$.

A direct comparison of the test data in Figs. 5(a) and 6(a) shows that the major disagreement between the hot jet case and the cold jet case is the considerable upward shift of the effective wall temperature with increasing inclination for the former. Fig. 6(a) demonstrates that the $\beta = 30°$ curve has largest θ values at all lateral points along the y-axis, followed by $\beta = 45°$ and $\beta = 90°$ curves, respectively. This is contrary to the slight descend of the effective wall temperature with increasing inclination in the cooling jet case. The higher θ values in the heating jet case correspond to higher wall temperatures on the target plate, implying that there is a significant temperature jump at all points along the y-axis with increasing inclination.

Fig. 6(b) illustrates how the effective wall temperature varies with inclination when heat is transferred from the jet flow to the target plate. The uphill shift of the actual stagnation point as well as the effective wall temperature is schematically drawn as observed in Fig. 6(a). Similar to the cooling jet case, there exists a crossing point on the uphill side between the effective wall temperature curves corresponding separately to the normal and oblique impinging jets. Let the lateral distance of the crossing point from the geometrical stagnation point be denoted as $y_{c,up}$. For the 45° inclination case, its location is about $y/D_h = +4$. On the other hand, whether or not there exists a crossing point on the downhill side is unclear from the present measurement data.

The upward shift of the local effective temperature with increasing inclination (from normal impingement) is further highlighted by plotting the value of θ at the geometrical stagnation point as a function of β for both cooling and heating jets, as shown in Fig. 7.

For a cooling jet, the apparent shifting of the peak of θ towards the uphill side causes the effective temperature at the geometrical stagnation point ($y/D_h = 0$) to decrease with increasing inclination. The value of θ at $y/D_h = 0$ on the target plate is reduced from 0.164 for $\beta = 90°$ to 0.122 for $\beta = 30°$. On the other hand, for a heating jet, although the actual stagnation point is also shifted towards the uphill side, the value of θ at the geometrical impingement point increases with increasing inclination. The effective wall temperature increases by nearly 29.6% when the inclination angle varies from 90° to 30°. Consequently, although the flow fields remain unchanged (Fig. 2), the heat transfer characteristics of a heating jet differ significantly from those of a cooling jet.

To examine the reasoning behind the opposite responses of local wall temperature to inclination between the hot and cold jets, consider next the measured velocity profile at a selected lateral

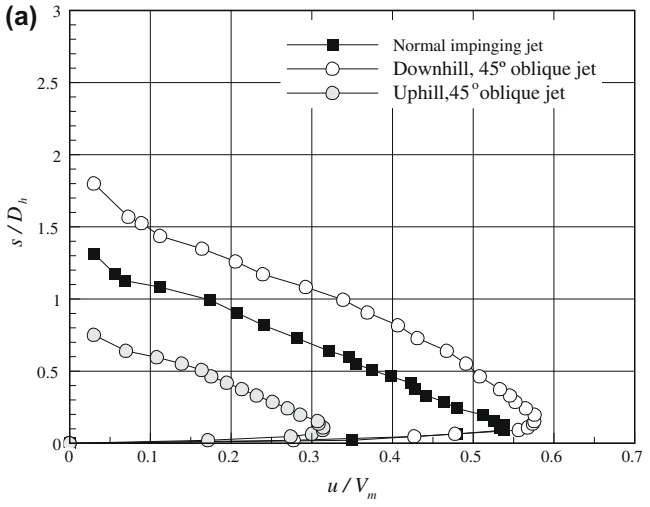

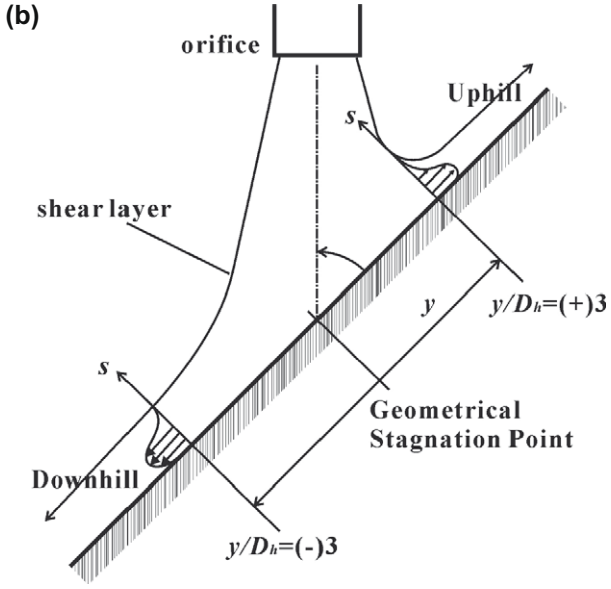

Fig. 8. Variation of momentum boundary layer thickness on uphill and downhill sides due to inclination: (a) measured velocity profile at $y/D_h = \pm 3$ and (b) schematic illustration, where s is the axis normal to the target plate.

location (e.g., $y/D_h = \pm 3$) traversed normal to the target plate, as shown in Fig. 8(a).

For normal impingement ($\beta = 90°$), following the terminology used by Nizou [14], one sees from Fig. 8(a) that the inner layer (or boundary layer) lies within $s/D_h = 0.13$ whilst the outer layer (or jet region) has a thickness of about $s/D_h = 1.6$. For oblique impingement ($\beta = 45°$), the outer layer on the uphill side of the target plate becomes thinner than that at the corresponding lateral location on the downhill side, a finding consistent with that reported in [11]. In comparison with the normal impingement case, the outer layer on the downhill side is thicker, whereas that on the uphill side is thinner. Integrating the velocity along the axis normal to the plate (the s-axis) at a fixed lateral location ($y/D_h = \pm 3$) for each case would give indication as to how the momentum of jet flow is redistributed due to plate inclination. The measured velocity profiles of Fig. 8(a) suggest that as the inclination is increased (relative to normal impingement), upon bifurcation of the impinging flow at the geometrical stagnation point, the jet flow with a higher momentum convects to the downhill side whereas that with a lower momentum is directed to the uphill side.

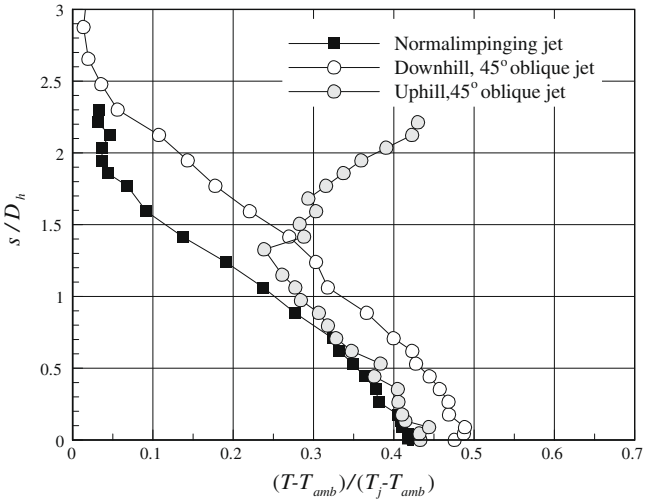

Fig. 9. Variation of thermal boundary layer thickness measured at $y/D_h = \pm 3$ where s is the axis normal to the target plate regardless of inclination.

Fig. 8(b) schematically summarizes the above observation. The thickening of both the outer and inner layers on the downhill side is associated with the increase in momentum of flow as a result of plate inclination. Correspondingly, due to conservation of momentum, the momentum on the uphill side is reduced.

It is interesting to notice that on the uphill side, the local wall temperature is as high as that of the normal impinging jet case, even though the jet flow has less momentum (Figs. 6(a) and 8(a)). To elaborate this feature, the local fluid flow temperature in a hot impinging jet was traversed along the s-axis at $y/D_h = \pm 3$ in a way similar to the velocity profile measurement. Fig. 9 plots the measured temperature profiles for both the normal impinging jet case and the 45° inclination case.

At the uphill side for $\beta = 45°$, the local fluid temperature is slightly higher than that of the normal impinging case. In addition, the increase in flow temperature above $s/D_h = 1.3$ is due to the fact that, along the transverse plane at $y/D_h = 3$, the temperature probe measures temperature of the hot jet flow (above $s/D_h = 1.3$) as well as that of the wall jet on the uphill side of the plate (below $s/D_h = 1.3$), as illustrated in Fig. 8(b). As noticed earlier, lesser momentum is available for this side of the target plate. One needs therefore to consider the influence of entrainment on heat transfer between the jet flow and the plate. The entrainment may be affected by two factors: (i) boundary layer (or inner layer and outer layer) thicknesses, and (ii) availability of air for entrainment. Abundant air for entrainment and thin boundary layer lead to maximum entrainment due to easiness in penetration of the surrounding air through the reduced boundary layer thickness. However, the above mentioned two factors (air availability and ease in boundary layer penetration) compete against each other to diminish the degree of air entrainment in the present case.

For simplicity, it is assumed that the flow field and hence the entrainment are predominantly two-dimensional along the y- and z-axes such that the contribution of flow along the x-axis to air entrainment is negligible. Whilst the downhill side of the plate experiences an increase in air availability for entrainment, the thickening of the boundary layer as well as the increased flow momentum tries to nullify this effect. Fig. 9 suggests that the later effect dominates as obtained results for both the thermal (Fig. 9) and momentum (Fig. 8(a)) boundary layers exhibit a similar trend, namely, a "right-ward shift" of the graph corresponding to the oblique impingement case along the z-axis relative to that in the normal impingement case (which we define as the increase in the z-axis values for all the corresponding y values). The combination of all these factors leads to increased effective wall temperature.

On the other hand, the uphill side has a thinner boundary layer than that on the downhill side, which should enhance the penetration of air entrainment and hence lead to a lower wall temperature. However, the overall entrainment of air on the uphill side is compromised due to the decreased volume of local air available, due to blockage by the target plate (which is inclined towards the uphill side). This leads to a net decrease in entrainment which in turn increases the wall temperatures or, equivalently, the effective temperature. Consequently, for the oblique impingement case, there is no "left-ward shift" of the thermal boundary layer (Fig. 9) as expected from the "left-ward shift" of the momentum boundary layer relative to the normal impingement case (Fig. 8(a)).

Consequently, for an obliquely impinging jet, the wall temperatures on both the uphill and downhill sides are higher than those of the normal impingement case. This explains the upward shift of the effective temperature over the entire lateral range considered in the present study when the hot jet is obliquely impinging on the target plate.

3.3. Two-dimensional versus three-dimensional hot jets

Contrary to what is observed in the present study for heated two-dimensional (2-D) air jets, existing data for heated circular air jets [5] or circular flame jets [8] reveal that the temperature and heat transfer coefficients all decrease with inclination. However, there is an apparent difference between a circular hot jet and a slot hot jet. The circular jet possesses substantially different entrainment effects in comparison with those associated with the slot jet. The entrainment in the circular jet is three-dimensional (3-D) whereas that in the slot jet is 2-D. Hence, the entrainment of flow along the x-axis is also significant in the circular jet case. As a result, the compromise of air availability on the uphill side is diminished whilst the increase of air availability on the downhill side is further augmented. Consequently, when the target plate is inclined relative to the jet orifice, even though the entrainment along the y- and z- axes is altered as previously discussed, the effect is minimized by the x-axis entrainment in the case of a circular jet.

4. Practical significance

Obliquely impinging slot jets have been widely used in industrial applications for cooling as well as heating. Contrary to common expectation, the two cases are significantly different in terms of heat transfer characteristics. The inclination of a cooling jet from the normal impinging position reduces the effectiveness of heat transfer between the jet and the target plate. Whilst the inclination leads to a more uniform distribution of wall temperature on the downhill side, it causes a higher temperature gradient on the uphill side. Conversely, for a heating jet, the inclination enhances the overall heat transfer performance of the jet. In automotive applications, for example, the inclination of a defrost nozzle relative to the windshields would be beneficial for ice removal in severe winter conditions.

5. Conclusions

A comparative experimental study of obliquely impinging heating and cooling slot jets has been carried out to explore the difference between their flow and heat transfer characteristics. It is demonstrated that the entrainment of ambient air plays a crucial role in the two-dimensional heating jet case.

The lateral distribution of effective wall temperature is similar for both the cooling and heating jet flows, with the point of maximum heat transfer shifted towards the uphill side of the target plate. However, for a heating jet, the upwards shift with inclination

occurs at all lateral positions. For a cooling jet, there is a slight decrease in effective wall temperature along the target plate, which is consistent with the decrease of Nusselt number observed in the literature for a similar experimental setup.

The upward shift of effective wall temperature in the heating jet case may be attributed to the reduction in effective entrainment of air on both the uphill and downhill sides of the target plate. The increase in effective wall temperature at all lateral points with inclination suggests that the heating jet is more effective for heat transfer than a cooling jet is. The effective wall temperature at the stagnation point increases by as much as 29.6% as inclination is increased. However, this effect may not be observed in an obliquely impinging circular heated air or flame jet because both have 3-D jet flow fields.

Acknowledgments

This work is supported by the National Basic Research Program of China (2006CB601203), the National Natural Science Foundation of China (50676075, 10632060 and 10825210), the National 111 Project of China (B06024) and the National High Technology Research and Development Program of China (2006AA03Z519).

References

[1] E.M. Sparrow, B.J. Lovell, Heat transfer characteristics of an oblique impinging circular jet, J. Heat Transfer 102 (1980) 202–209.

[2] A.H. Beitelmal, M.A. Saad, C.D. Patel, The effect of inclination on the heat transfer between a flat surface and an impinging two-dimensional air jet, Int. J. Heat Fluid Flow 21 (2000) 156–163.

[3] Y.E. Akansu, M. Sarioglu, K. Kuvvet, T. Yavuz, Flow field and heat transfer characteristics in an oblique slot jet impinging on a flat plate, Int. Commun. Heat Mass Transfer (2008), doi:10.1016/j.icheatmasstransfer.2008.03.005.

[4] X. Yan, N. Saniei, Heat transfer from an obliquely impinging circular air jet to a flat plate, Int. J. Heat Fluid Flow 18 (1997) 591–599.

[5] R.J. Goldstein, K.A. Sobolik, W.S. Seol, Effect of entrainment on the heat transfer to a heated circular air jet impinging on a flat surface, J. Heat Transfer 112 (1990) 608–611.

[6] J.W. Baughn, A.E. Herchanova, X. Yan, An experimental study of entrainment effects on the heat transfer from a flat surface to a heated circular impinging jet, J. Heat Transfer 113 (1991) 1023–1025.

[7] S.A. Striegl, T.E. Diller, The effect of entrainment temperature on jet impingement heat transfer, J. Heat Transfer 106 (1984) 27–33.

[8] K.P. Perry, Heat transfer by convection from a hot gas jet to a plane surface, Proc. Inst. Mech. Eng. 168 (1954) 775–780.

[9] H.W. Coleman, W.G. Steele, Experimentation and Uncertainty Analysis for Engineers, second ed., Wiley, New York, 1999.

[10] B. Ertan, Confined impinging air jet at low Reynolds numbers, Exp. Therm. Fluid Sci. 19 (1999) 27–33.

[11] H.M. Hofmann, M. Kind, H. Martin, Measurements on steady state heat transfer and flow structure and new correlations for heat and mass transfer in submerged impinging jets, Int. J. Heat Mass Transfer 50 (2007) 3957–3965.

[12] B.R. Holloworth, S.I. Wilson, Entrainment effects on impingement heat transfer: part I. Measurements of heated jet velocity and temperature distributions and recovery temperatures on target surface, J. Heat Transfer 106 (1984) 797–803.

[13] V. Narayanan, J. Seyed-Yagoobi, R.H. Page, An experimental study of fluid mechanics and heat transfer in an impinging slot jet flow, Int. J. Heat Mass Transfer 47 (2004) 1827–1845.

[14] P.Y. Nizou, Heat and momentum transfer in a plane turbulent wall jet, J. Heat Transfer 103 (1981) 138–140.